ORNL/TM

Cooperative Research and Development Agreement Final Report for Cooperative Research and Development Agreement Number ORNL00-0601

HALLIBURTON COMPOSITE BRIDGE PLUG ASSEMBLY

ORNL/TM

Metals and Ceramics Division

Cooperative Research and Development Agreement Final Report for Cooperative Research and Development Agreement Number ORNL00-0601

Halliburton Composite Bridge Plug Assembly

J. M. Starbuck, C. R. Luttrell, and G. Aramayo
Oak Ridge National Laboratory, Oak Ridge, TN 37831-6053

January 2005

Prepared by the
Oak Ridge National Laboratory
Oak Ridge, Tennessee 37831-6053
Managed by UT-Battelle, LLC
for the
U.S. DEPARTMENT OF ENERGY
under contract DE-AC05-00OR22725

TABLE OF CONTENTS

LIST OF FIGURES

LIST OF TABLES

ABSTRACT

The overall objectives of this CRADA were to assist Halliburton in analyzing a composite bridge plug and to determine why their original design was failing in the field. In Phase 1, finite element analyses were done on the original composite slip design and several alternative designs. The composite slip was the component in the bridge plug that was failing. The finite element code ABAQUS was used for these calculations and I-DEAS was used as the pre- and post-processor in the analyses. Several different designs and materials were analyzed and recommendations were made towards improving the design

In Phase 2, the objective was to develop finite element models that would accurately represent the deformations in the entire all-composite 4-1/2" diameter bridge plug assembly. The finite element code LS-DYNA was used and the results from this effort were intended to expand Halliburton's composite design and analysis capabilities with regard to developing future composite components for downhole tools. In addition to the finite element modeling, this effort involved the utilization of micromechanics to determine the necessary composite material properties that were needed as input for finite element codes.

1. PHASE ONE

1.1 COMPOSITE SLIP ORIGINAL DESIGN

The original design of the composite bridge plug for the Halliburton program was failing in the field. Finite element analyses were done on the original design and several alternative designs. The finite element code ABAQUS was used for these calculations. I-DEAS was used as the pre- and post-processor in the analyses. Two different loading conditions were considered. One is called the top slip and the other is called the bottom slip. It was determined that the bottom slip case was the one that was failing, so most of the calculations were done using this loading. Several different designs and materials were analyzed to find the best solution to the problem.

The two loading conditions consisted of different loads and boundary conditions on the plug and pins. The top slip case was loaded with a force of 39,760 lbs. applied to a rigid surface on the back flat of the plug. The plug was fixed along the bottom sloped region with a rigid surface and the pins inserted into the plug were fixed along highest edge of the pins. The bottom slip case was free on the back flat and loaded along the sloped bottom with a force of 105,208 lbs. applied to a rigid surface in the direction parallel to the top surface. The pins were again fixed at the top.

The original design was analyzed with both load cases to evaluate what was actually occurring. The results of these calculations showed that the wedge would fail under the bottom slip load case. The material properties used for the wedge for this case were:

E_1 = 3.4624E06 psi
E_2 = 3.4624E06 psi
E_3 = 1.4494E06 psi
ν_{12} = 0.0975
ν_{13} = 0.2917
ν_{23} = 0.2917
G_{12} = 0.5172E06 psi
G_{13} = 0.5239E06 psi
G_{23} = 0.5239E06 psi
In-plane tensile strength = 75,000 psi
In-plane compressive strength = 75,000 psi
Out-of-plane tensile strength = 4,000 psi
Out-of -plane compressive strength = 20,000 psi
Shear strength = 14,000 psi

The material property used for the Boron carbide pins were:

E = 42.0E06
ν = 0.29

The results of the original design loaded with the top slip condition showed that the composite plug should withstand this loading configuration. Figure 1 shows the stress in the plug in the direction perpendicular to the direction of the layers (out-of-plane). Since this is the direction of the lowest tensile and compressive strengths it is the direction most likely to show failure first. The results show some very localized areas exceeding the out-of-plane limits, but these are in locations where the pins were attached to the plug. The constraints placed on this attachment were that they were completely tied together. This is over constrained compared to the real case and gives higher than actual stresses. The maximum stress in the in-plane directions is about 45,000 psi, and this is also located in the region where the pins attach to the plug. This is well below the allowable of 75,000 psi.

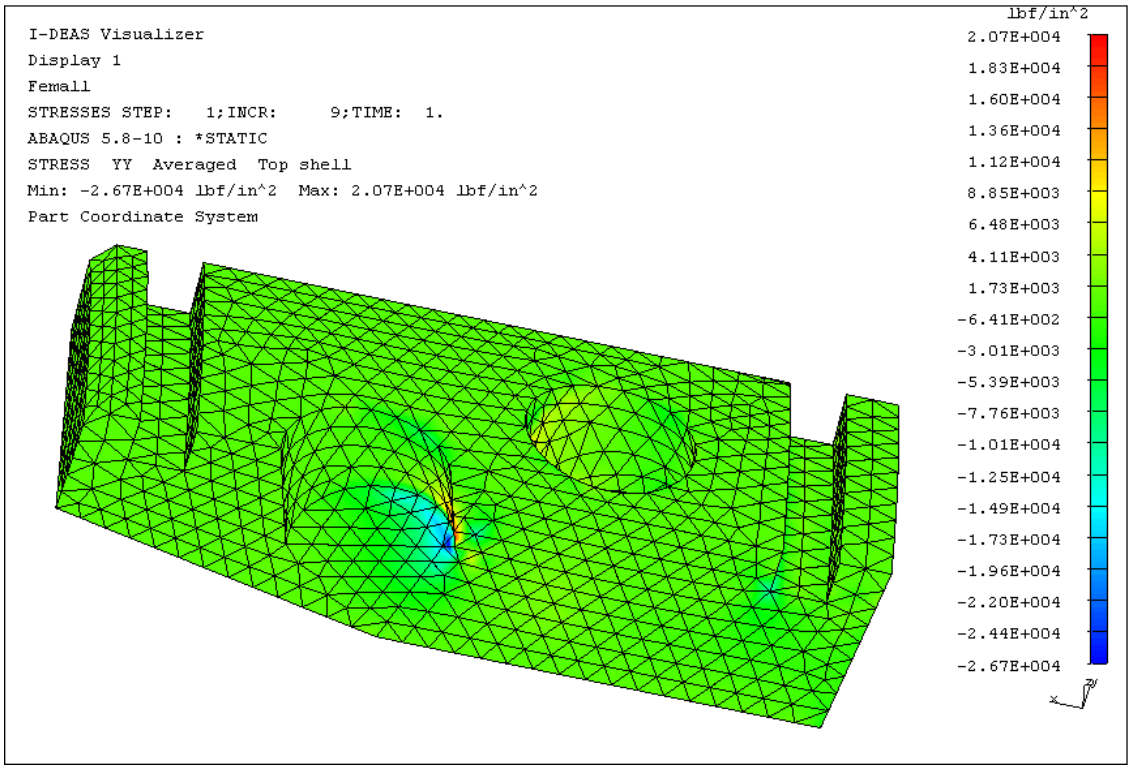

Figure 1. Out-of-Plane Stresses for Top Slip Case.

The results of the original design loaded with the bottom slip condition showed that the composite plug would fail under these conditions. This analysis showed that the stresses exceed the allowable strengths in the direction normal to the surface of the wedge and in the shear direction. The large force applied to the sloped region of the wedge and the fixed boundary condition on the pin above the slope caused a large out-of-plane stress. Figure 2 shows the regions in the model that are above the allowable limits in the out-of-plane direction and the magnitude of these stresses. This figure shows that the failure in the out-of-plane direction is over a large region surrounding the front hole and bottom sloped region. Figure 3 shows the region that fails in the shear direction.

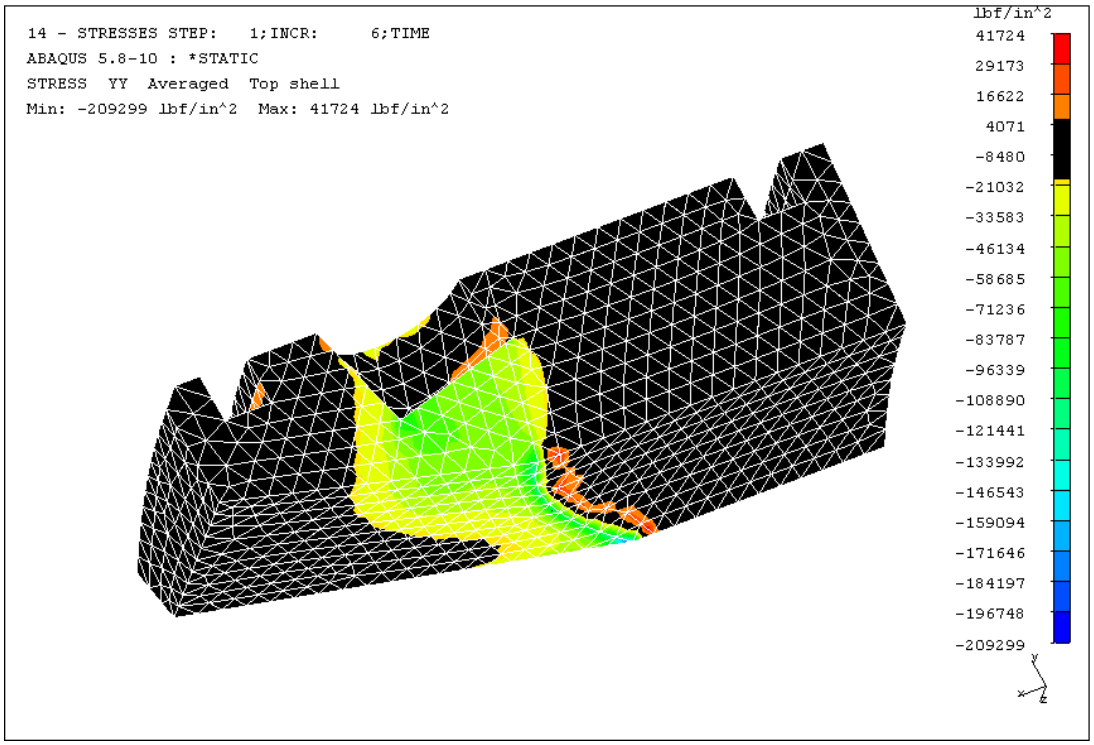

Figure 2. Out-of-Plane Failed Region in Bottom Slip Case.

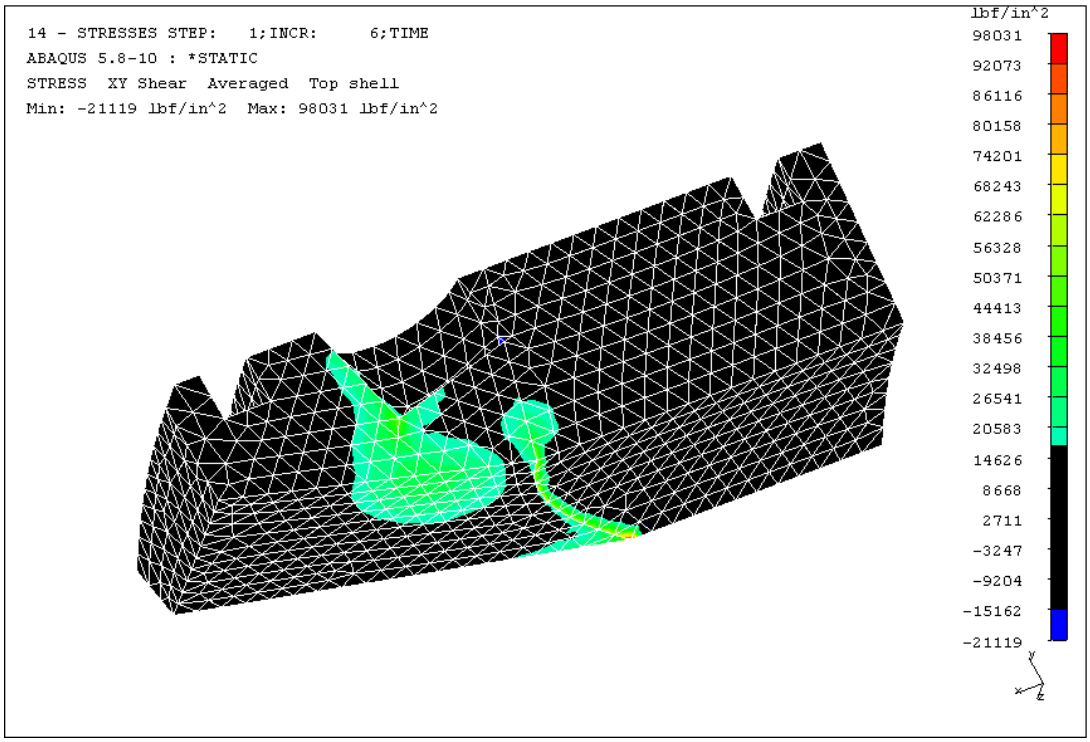

Figure 3. Shear Stress Failed Region in Bottom Slip Case.

1.2 COMPOSITE SLIP DESIGN MODIFICATIONS

One design change that was considered was to change the angle of the slope on the plug from 14 degrees to 7 degrees to thicken the section between the applied load and the fixed boundary condition. The results of this analysis showed that this change does not effect the out-of-plane stress much, but it does reduce the shear stress. By comparing Figure 4 and Figure 2 it can be seen that there is little affect on the out-of-plane stresses. Figure 5 shows that the shear stress is reduced.

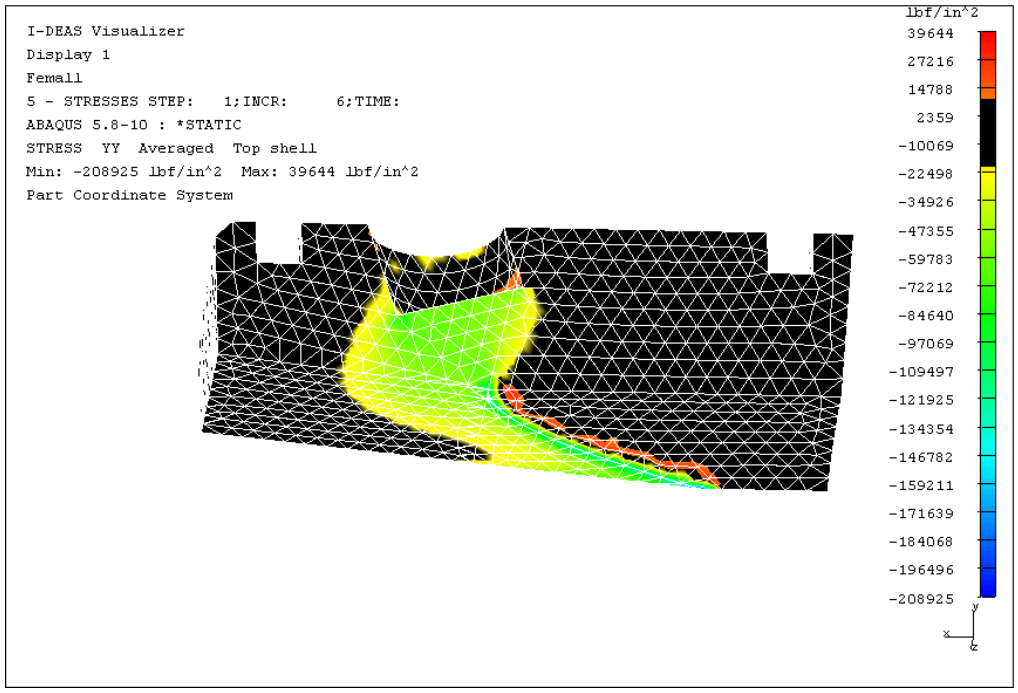

Figure 4. Out-of-Plane Stress with 7 Degree Sloped Region.

After considering that to reduce the out-of-plane stress, the cross section of the area under the load needed to be increased, a model was analyzed with a groove across the top of the plug in the front instead of the pin. This spread out the reaction forces caused by the fixed boundary conditions on the pin and reduced the out-of-plane stress. The results of this analysis are shown in Figure 6. Although the stresses were reduced, they are still above the allowable limits for the material. It was determined that a new material needed to be used to make the plug.

The original design was reanalyzed using a chopped carbon fiber reinforced sheet molding compound with the following properties:

E = 6.5E06 psi
ν = 0.3
Tensile strength = 43,500 psi
Compressive strength = 58,000 psi
Shear strength = 14,000 psi

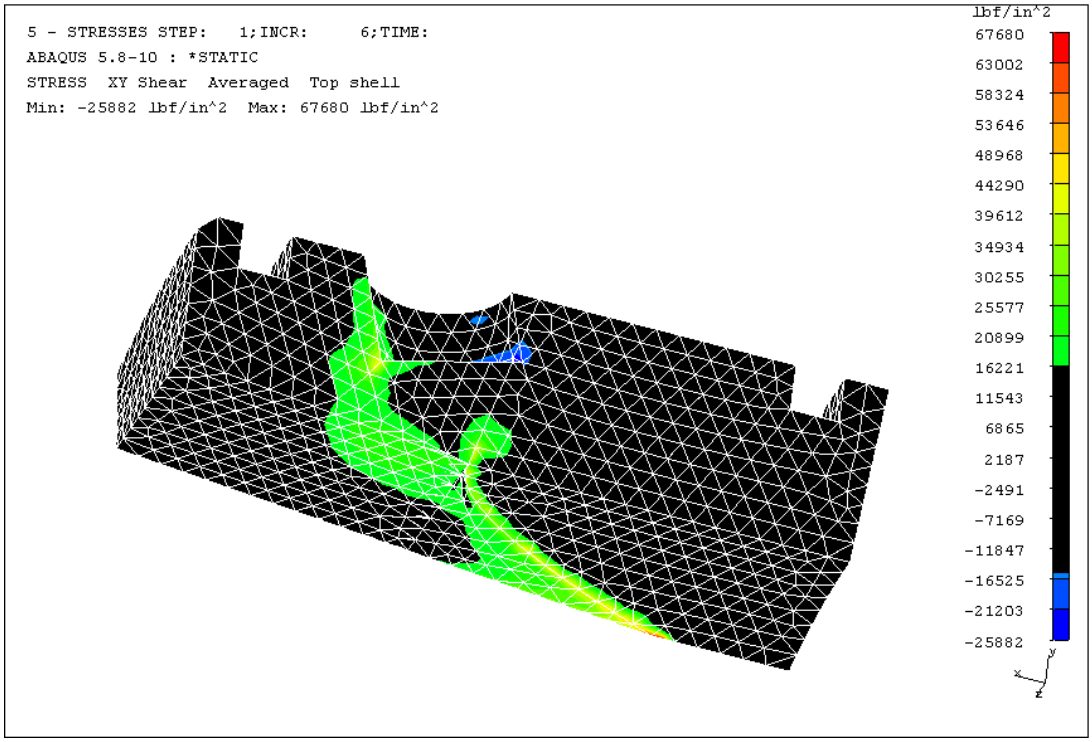

Figure 5. Shear Stress Failure Region with 7 Degree Slope.

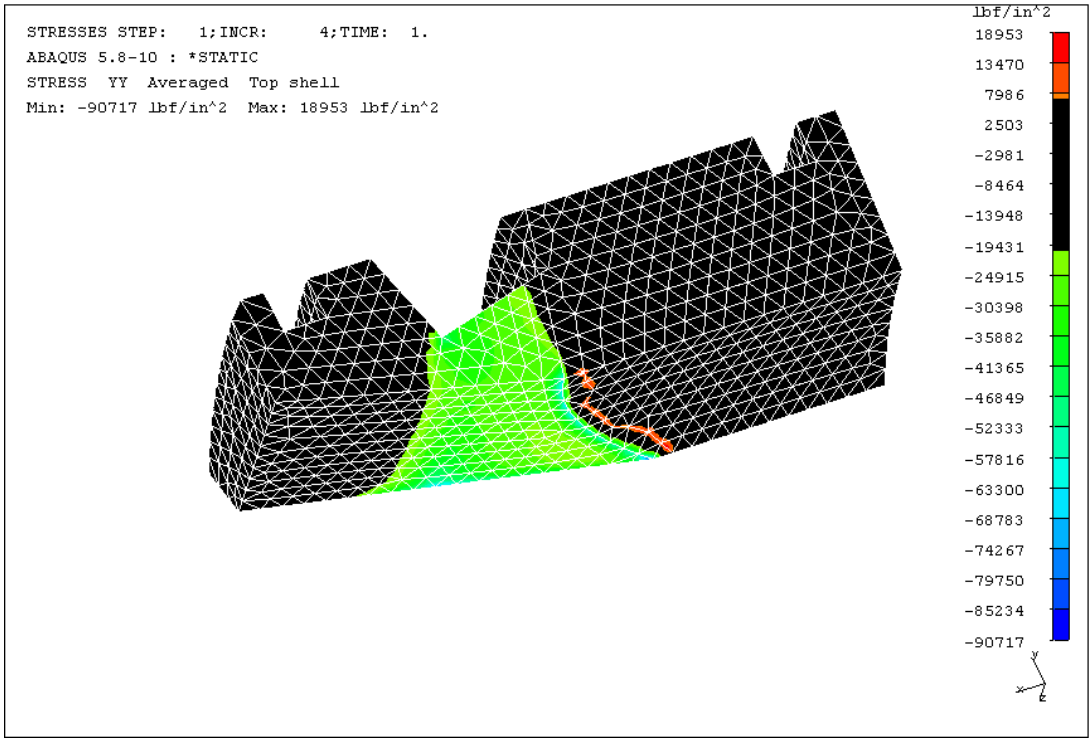

Figure 6. Out-of-Plane Failure Region with Groove.

The material for the pins remained the same as before. The results of this analysis showed that with the new material the out-of-plane stress is only above the limits in a localized region along the bottom boundary where the sloped region begins and immediately under the pin as shown in Figure 7. For this case the shear strength is the dominating stress to consider. The shear stress is the primary stress exceeding the allowable limits as can be seen in Figure 8. The maximum shear stress is 132,100 psi. Although the peak value is in a localized region, there is a significant region exceeding the limit.

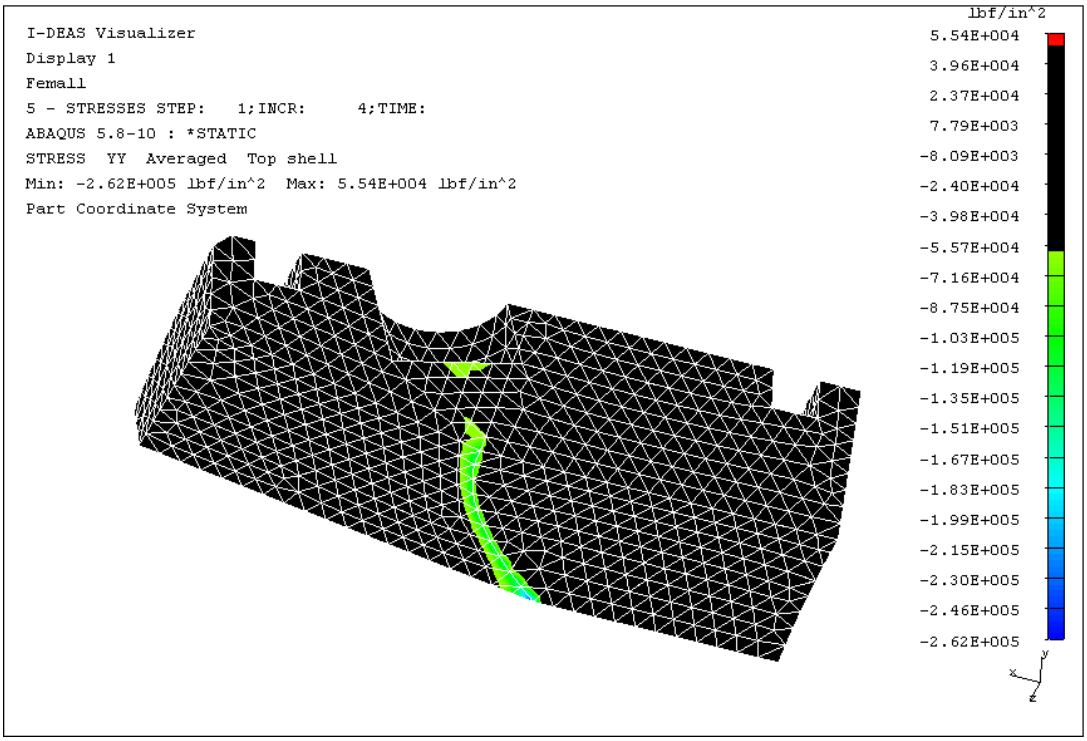

Figure 7. Out-of-Plane Failure Region with New Material.

The design with the groove replacing the pin in the front of the plug was analyzed using the new material properties. The results of this calculation showed that the wedge exceeds the allowable limits through the thickness only along a very small band at the boundary of the sloped region. Again with this case the primary stress exceeding the allowable limits is the shear stress. Figures 9 and 10 show the results of this analysis. The maximum shear stress for this case is 56,102 psi. This is considerably lower than the value shown in Figure 8, but there is still a significant region exceeding the allowable limit.

To reduce the shear stress a model was analyzed with the groove in the front and the 7 degree slope, instead of the original 14 degree slope. The results of this analysis are shown in Figures 11 and 12. For this case, as in the case above, the out-of-plane stress is not the problem. The maximum shear stress is reduced to 38,500 psi. This is still above the allowable limit in a portion of the slope region.

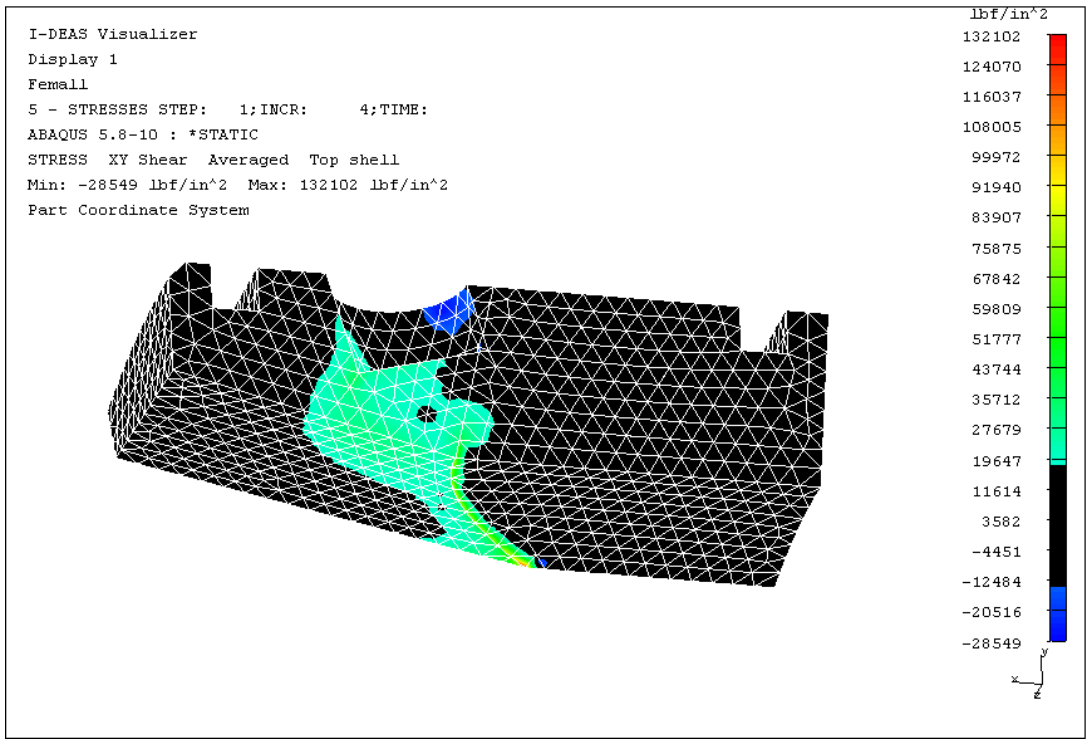

Figure 8. Shear Stress Failure Region with New Material.

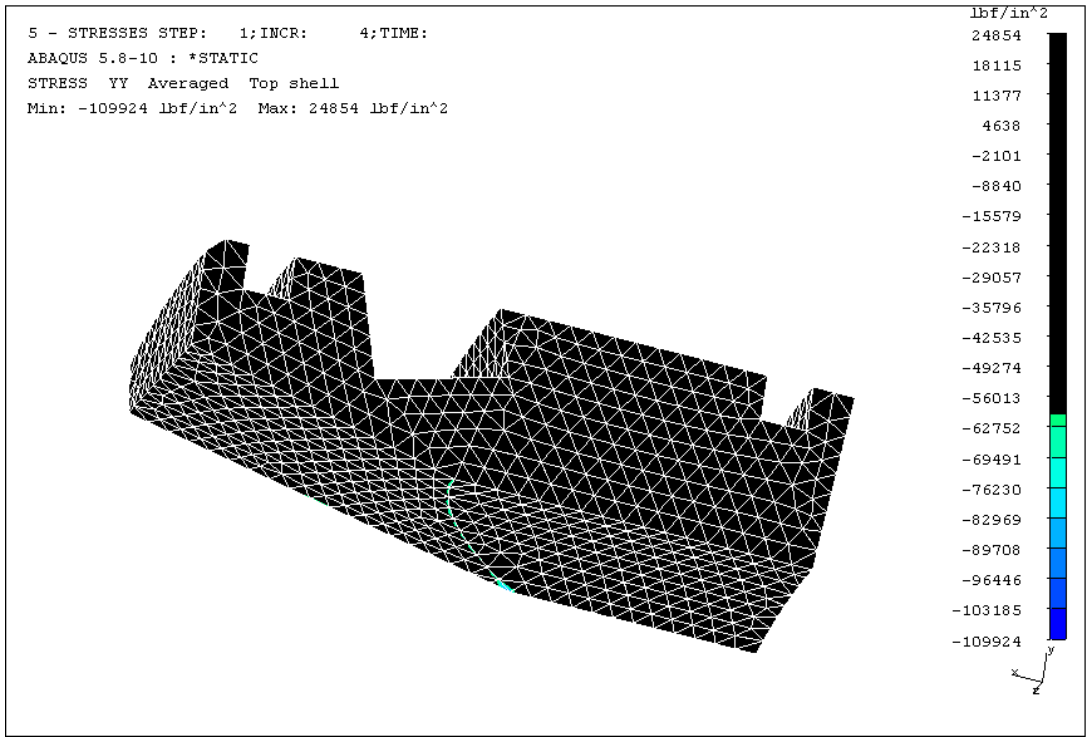

Figure 9. Out-of-Plane Failure Region, Groove with New Material.

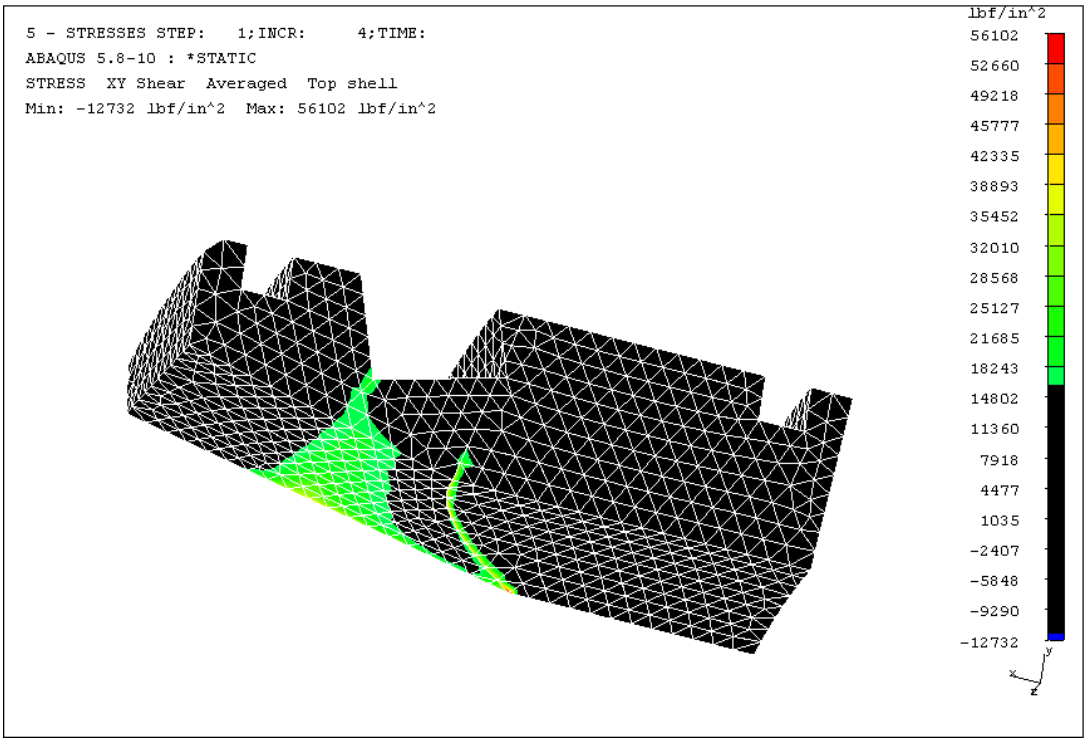

Figure 10. Shear Stress Failure Region, Groove with New Material.

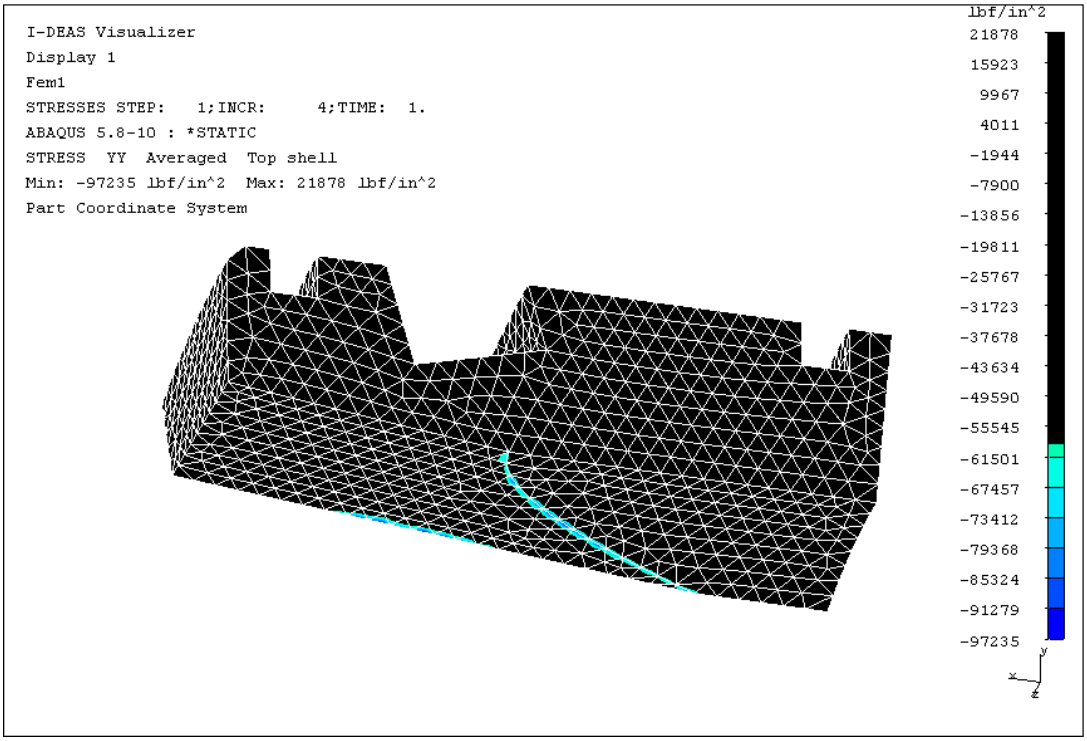

Figure 11. Out-of-Plane Failure Region, 7 Degree Slope and New Material.

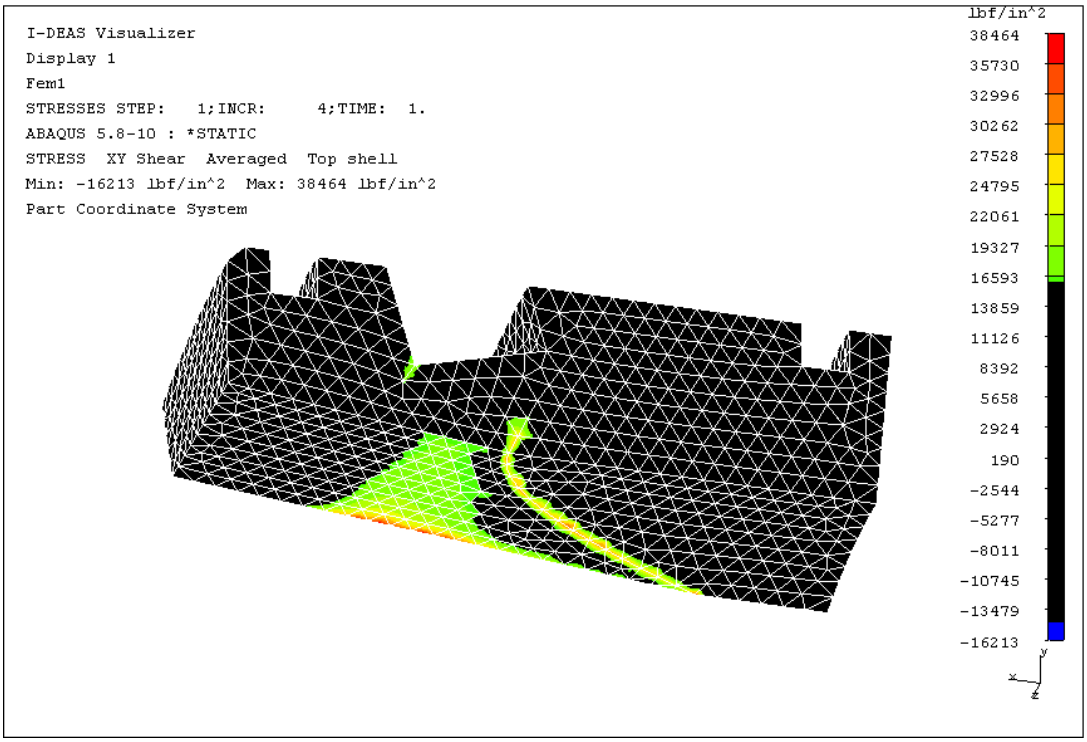

Figure 12. Shear Stress Failure Region, 7 Degree Slope and New Material.

The results of these analyses showed that by modifying the present design and using a new material the stresses in the wedge could be reduced to values that are close to the allowable limits for the new material. Slight modification to the groove in the front of the plug and other parts of the plug could bring the stresses below the allowable limits. All of the models included a sharp corner where the slope on the bottom of the plug begins. Including a radius in this area would reduce the localized stresses in this region.

2. PHASE TWO

2.1 COMPOSITE BRIDGE PLUG ASSEMBLY ANALYSIS

The objective of this work was to develop finite element models that would accurately represent the deformations in an all-composite 4-1/2" diameter bridge plug. The results from this effort are intended to expand Halliburton's composite design and analysis capabilities with regard to developing future composite components for downhole tools. In addition to the finite element modeling, this effort involved the utilization of micromechanics to determine the necessary composite material properties that are needed as input for finite element codes.

2.1.1 Finite Element Model Development

A finite element model of the composite bridge plug has been completed, where the model corresponds to the general outline shown in Figure 13 and in Dwg. No. 803.94599. The finite element model was developed using the computer program TRUGRID. The model geometry was based on the drawings given in Table A1 of Appendix A and developed for input to LS-DYNA using a quasi-static mode of operation.

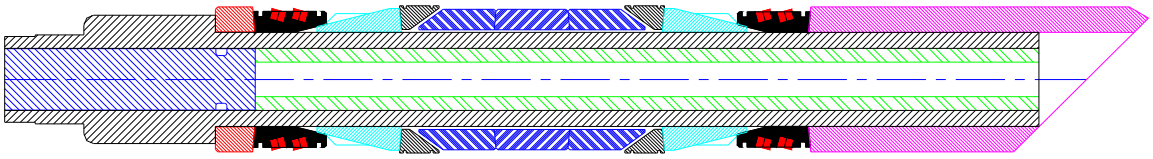

Figure 13. Sketch of composite bridge plug cross-section.

Initially, two models were developed to assess the sensitivity of the system response to geometric configurations of the wedge-slip ring and ring spacer that are shown in detail in Figure 14. In this figure, the slip ring is shown for two locations, in the first case a section of the ring is shown in contact with the wedge, this results in a configuration in which there is a gap between the slip ring and the ring spacer (at the right of the figure). In the second case the slip ring is in contact with the ring spacer creating a gap in front of the slip ring and the wedge. Because of the large ID formed by the segments of the slip ring, it appears that is not possible to achieve a stable configuration for both slip ring locations (before and after the rubber sections).

The models generated are described as follows. **Model a**- the gap described by the 'first case' in the above paragraph, has been filled with a spacer that has the ID equal to the OD of the main shaft, and is in contact with the ring spacer at one end and to the slip ring at the other end. This modification is made for both slip ring locations as shown in Figure 15. **Model b**- In this model the 'dummy inserts' that have been used in model a- are deleted and the slip rings are forced to be in contact with the wedges. This configuration is shown in Figure 16.

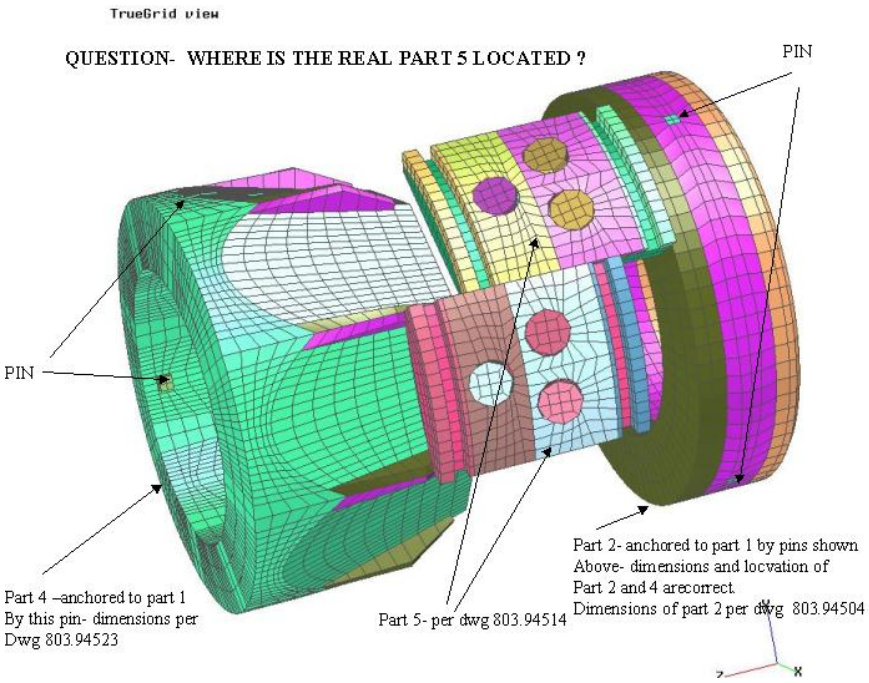

Figure 14. Details of wedge-slip ring finite element mesh.

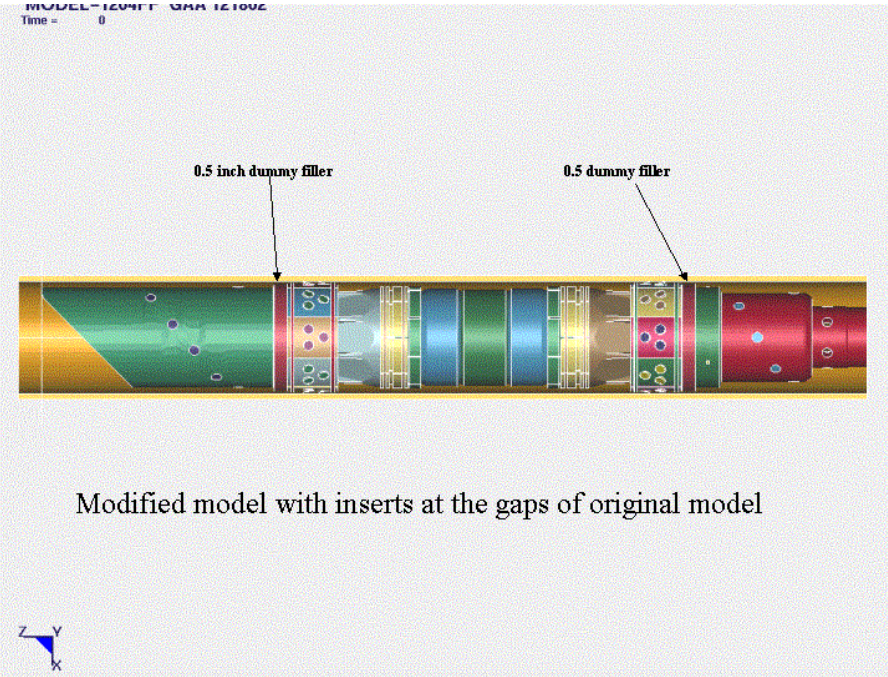

Figure 15. Model a.

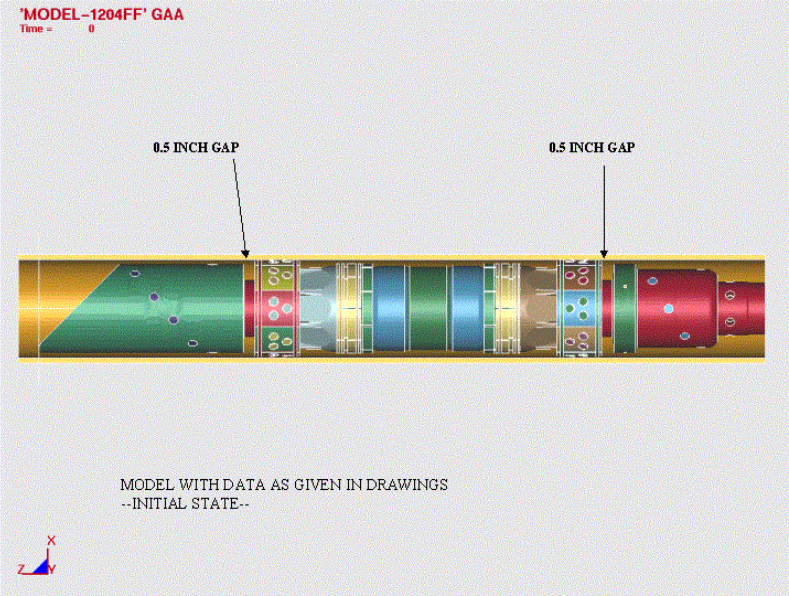

Figure 16. Model b.

The simulation of the system using either of the models described above is characterized by significant bending of the shaft that can be attributed to the non-symmetric point of contact of the mule shoe shown in the left-hand side of Figures 15 and 16. This bending results in a non-symmetric response of the rubber elements. Contact of the rubber and the casing occurs at one point before the remaining part of the rubber achieves contact with the casing.

The initial simulations had a long list of assumptions that are summarized below:

-Pressure loading: amplitude and duration

-Material properties: the analysis was performed using aluminum for most of the components, the Elastic modulus seems to be in the correct order of magnitude relative to some composite materials, the material is assumed to be elastic, and there is no yield stress in the formulation.

-The response of the pins that connect several components is also based on an assumed desired response. It has been assumed that the pins that connect the shoe to the shaft will fail at an equivalent strain of 14%. The remaining pins fail at higher loading.

-The outer casing is assumed to be elastic and is fully supported at the outer diameter.

Because of the large number of assumptions involved it was possible to achieve any desired response. One point that deserved attention and was modeled in considerable detail was the rubber-extrusion limiters-outer casing interface. There is a large sensitivity

to material data in the representation of the interface parameters that account for the contact at this location. Consequently, a separate model was developed in an effort to 'tune' the model interface parameters and this model is shown in Figure 17.

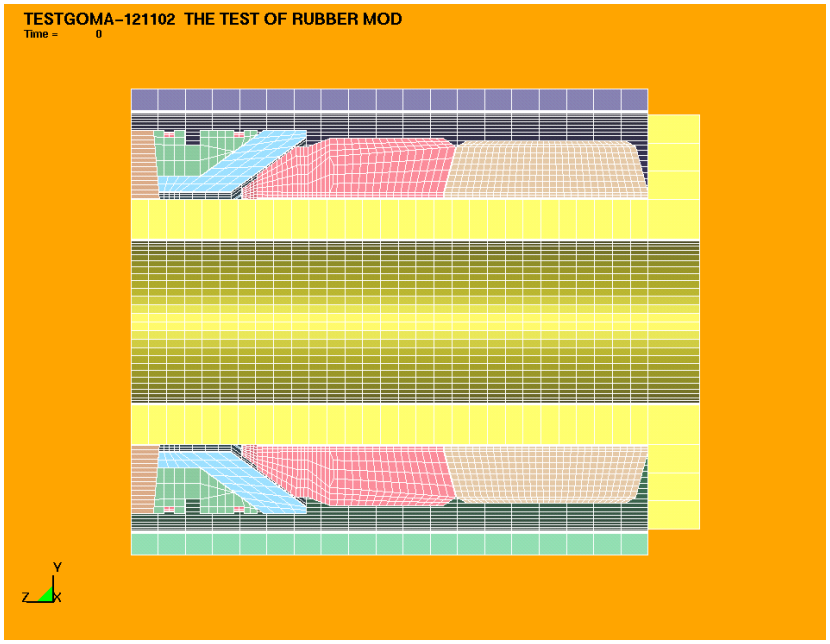

Figure 17. Interface parameters model.

In this model the entire section in front of the assembly that exists ahead of the extrusion limiters has been replaced by a piston that is free to travel along the shaft. The typical response of this model is given by the results shown in Figure 18.

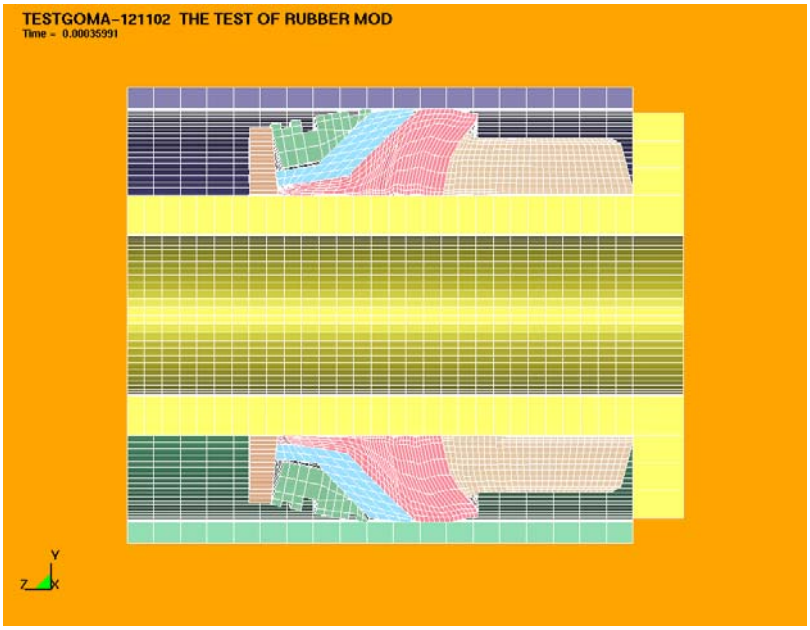

Figure 18. Characteristic response of outer rubber rings.

Figure 18 shows the characteristic response of the outer rubber rings that fill the cavity between the shaft and the casing. There is very little compliance between the center rubber sections. Numerically there were a large number of problems that had to be overcome to achieve this response. These problems were associated with the large discrepancy of the bulk moduli of the rubber and adjacent material. This affects the contact model that is based on a penalty method where the forces are derived from the material properties. The large deformations experienced by this model also resulted in large hour-glassing of the rubber elements. This numerical difficulty was also overcome for the model shown above. This model is good for an axi-symmetrical response of the rubber-shaft-casing, i.e. the situation where the shaft does not translate radially due to the imposed loading. Analysis of the entire assembly has shown, with the initial assumptions, there is bending of the shaft that results in radial displacements in the shaft with subsequent pinching on one side of the rubber rings.

To proceed with the modeling effort, it was required to simplify the model and to modify the kinematics such that the bending deformations were eliminated. Also, at this stage of the model development, composite material properties that would be representative of materials used for manufacturing an all-composite bridge plug were inserted into the analytical model.

A simplified model is shown in Figure 19. In this simplification, parts 1, 2, 3, and 4 were fused together, i.e., only one part and one material, all pins were removed and filled with material, all gaps between adjacent parts were removed, and the applied load consisted of a displacement input instead of a pressure loading. The magnitude of the prescribed displacement was derived from the overall reduction in length of the bridge plug after it has been set downhole.

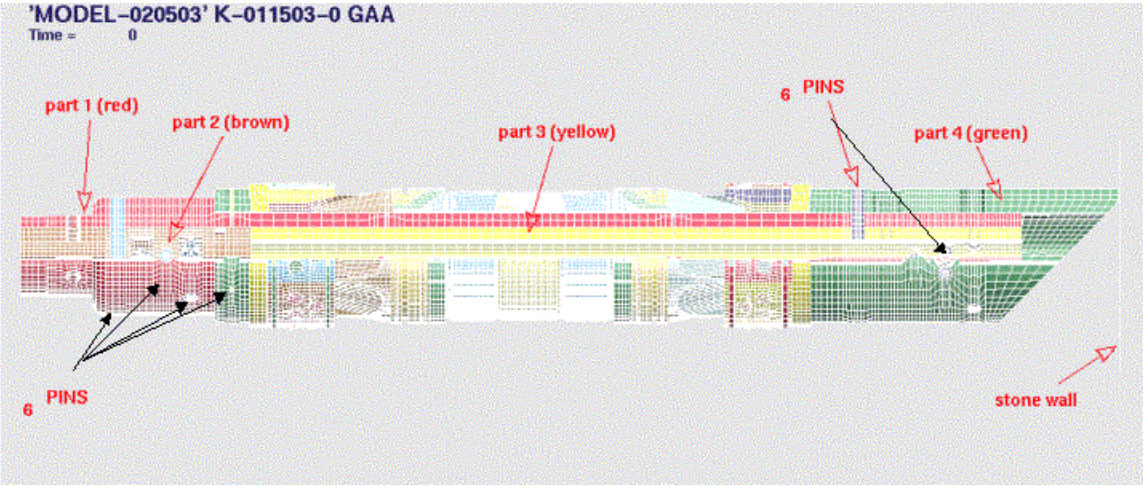

Figure 19. Simplified model.

The model has 49 material entities, 204945 nodal points, 163070 hexahedral elements, 956 single point nodal constraints, and 5 contact definitions. Using LS-DYNA in a quasi-static mode of operation, this is a displacement input class problem, where the

displacement of the mandrel is specified as a function of time while the ring spacer, part 2 in Table A1 is constrained in the axial direction.

The finite element model developed takes advantage of the symmetrical properties of the plug assembly. Figure 20 shows a view of the symmetrical half model developed for the analysis.

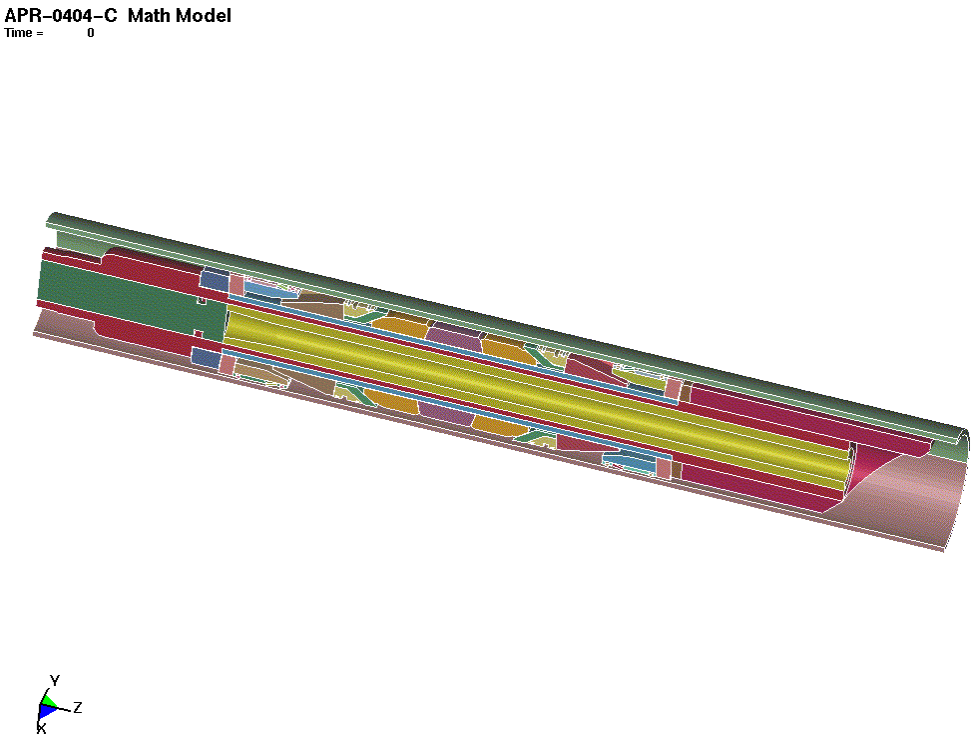

Figure 20. Finite Element Model of the Bridge Plug Assembly.

The material model used in the analysis corresponds to the bi-linear isotropic elastic-plastic material. The material properties for most of the components correspond to the fabric E-glass 1543 Woven model in Table 1. The isotropic material constants are: Young's Modulus of 3,637,000 psi, Poisson's ratio of 0.445, and density of 0.0515 lbs/in^3.

The extrusion ring assemblies are modeled using the bi-linear elastic plastic material model with the following material parameters: Young's Modulus: 4,300,000 psi, Poisson's ratio: 0.4, Yield stress: 17,500 psi with a tangent modulus of 0.0, and a material density of 0.07 lbs/in^3.

The mandrel (part 1, table A1), plug-bridging (part 9), shoe (part 8), are modeled as rigid components. These materials share nodes at their interfaces. Figure 21 shows the components that are rigid in the model. The displacement input is applied to the mandrel left side.

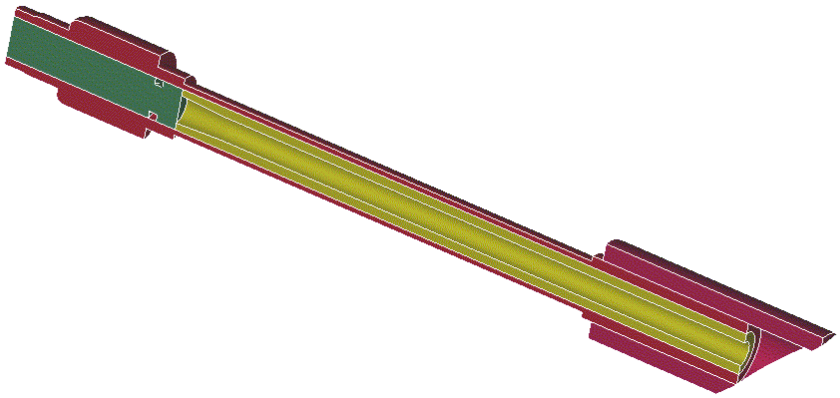

Figure 21. Rigid material components in the model.

The hard rubber components are modeled using the Mooney-Rivlin rubber material model in LS-DYNA. Two distinct sets of material parameters are used for the outer and center rubber rings. These data has been provided as input for the simulation. The center rubber ring has the constants: A=104.50 and B=24.57, while the end rings parameters are: A=153.50 and B=331.47. The material density has been estimated to be equal to the other woven materials. There is strong evidence that the material parameters for the end rubber components are in error.

Because of the disparity in the nodal locations between the outer, inner and pins in the slip composite rings, part 4 in Table A1, there is need to constrain the nodes within these components. There are 956 nodal constraints associated with this modeling scheme. Each set of the radial slip rings is free to slide independently. A typical ring assembly of these components is shown in Figure 22.

The retaining rings, parts 3 and 19 in Table A1, are also modeled as an elastic-plastic material model. These components have the added 'erosion' feature attached to the material definition, the failure criteria used for the deletion of elements that undergo failure at tension is based on an exceeding the maximum principal strains. The maximum plastic strain at failure is assumed to be 6%. This is an assumption based on the desired response of the components.

The casing is modeled as an elastic material where the material data is assumed to be comparable to A-36 carbon steel.

The displacement input to the mandrel is given in table form that specifies the maximum mandrel travel will occur at 0.0026 seconds from initiation of the event. This data is also an assumption for the analysis. For slower rate of loading, LS-DYNA has a mass scaling technique that basically scales up the material density of the components thus allowing longer runs at slower rates of motion. The time step that is a multiple of the smallest Courant step is specified and is kept constant regardless of the deformation introduced in the model. Attention should be given to not introducing large accelerations associated with large mass scaling time step analyses.

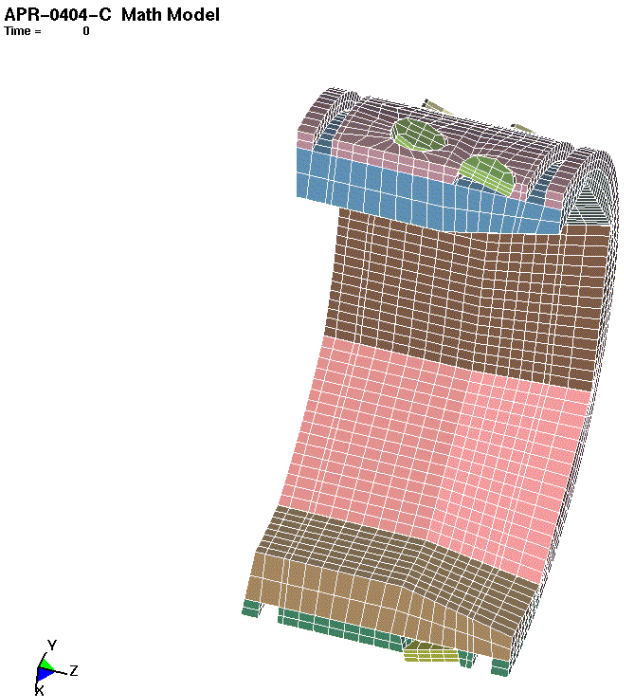

Figure 22. Left side symmetrical view of slip ring assembly.

Hourglass control is achieved using a scheme based on a stiffness formulation attributed to Flanagan-Belytshko, and based on an exact volume integration. Relative large hourglass coefficients are used because of the large deformation introduced to the rubber elements. Effects of bulk viscosity would probably reduce the magnitude of the hourglass coefficients and make the deformation better behaved.

The model is formed by the integration of independent components, each element is assigned a unique material name and integration is achieved physically by the retaining rings and the constraint provided by the casing. It is therefore necessary to specify a contact formulation that eliminates part penetration while maintaining continuity between the components.

The problem is highly sensitive to the model used for the contact definition in the analysis. This problem is partially attributed to relative soft materials that undergo large deformation. For the rubber-to-rubber (parts 7 in table A1), and rubber-to-moving-interface-part (parts 7, part 6 and 5 in Table A1) a surface-to-surface contact model is used. In this model a soft-contact penalty model with a low penalty parameter is used. Effects associated with constraints at the plane of symmetry are considered. The interface between the other components of the model is modeled using a global single-surface model formulation; in this model a soft constraint with low penalty constant is also used.

The contact models include a damping constant to minimize the ringing effects attributed to the forces generated to avoid part penetration.

The numerical simulation was performed under the assumptions given in previous paragraphs. The computation aspect was done using the explicit program LS-DYNA version 970-3535 installed in the IBM power 4 MPM computer installed at the ORNL site. A typical execution run was performed using 4 processors.

2.1.2 Finite Element Model Validation

Results of a simulation are compared against a single experimental set of results made available for this purpose. This experimental solution is given in terms of geometric changes ONLY, there is no information regarding stress or forces between the limiters and casing or in any other component of the model.

The experimental solution used to benchmark the numerical solution is given in the Halliburton Energy Services drawing CLO-803-945490. This drawing is not consistent with the input geometry used in the development of the finite element model. The 'slip' part (item 4 in Table A1) is different and there might be differences in the dimensions of the plug assembly.

The 'as assembled' cross section of the finite element model of the plug assembly is shown in Figure 23.

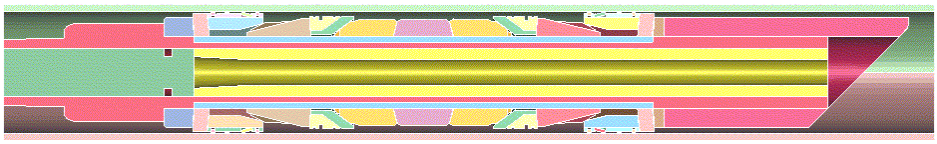

Figure 23. 'As assembled' Finite element model.

The 'deformed' cross section of the finite element model, after the mandrel undergoes the prescribe displacement input is shown in Figure 24.

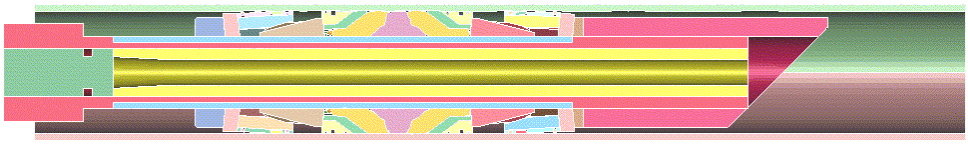

Figure 24. 'Deformed' configuration of finite element model of plug assembly

The time history input that is the ASSUMED displacement function for travel of the mandrel is shown in Figure 25. The units are seconds for time, and inches for displacement.

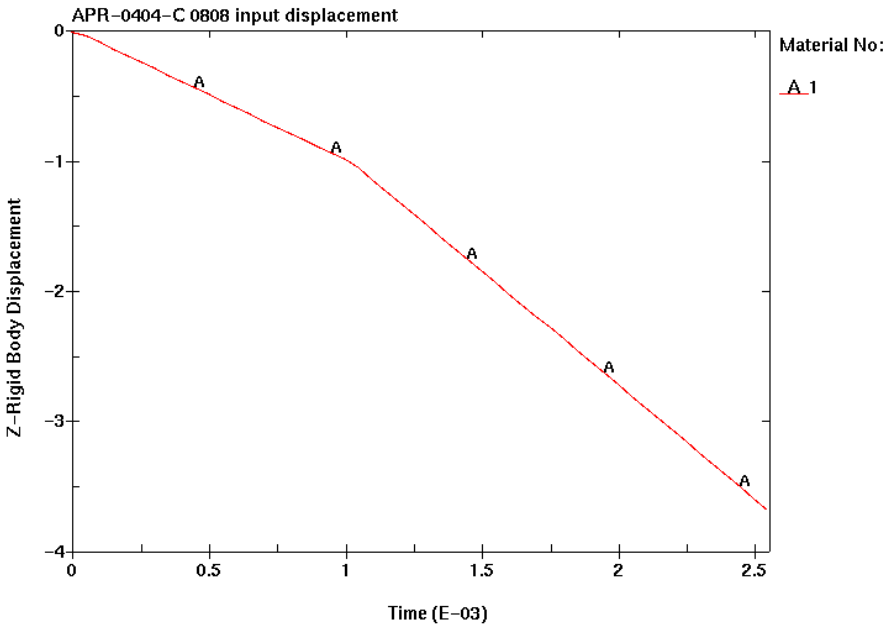

Figure 25. Assumed displacement input used in analysis.

A close-up of the region of interest for the 'as assembled' cross section is shown in Figure 26. This figure shows the two parameters that are the only information provided for validation purposes. The distance that exists between the 'wedges' (item 5 in Table A1) is denoted by the letter 'A'. The distance that exists at the outer boundaries of the 'end rubber components' or at the inside of the extrusion limiters (item 6 in Table A1) is denoted by the letter 'B'.

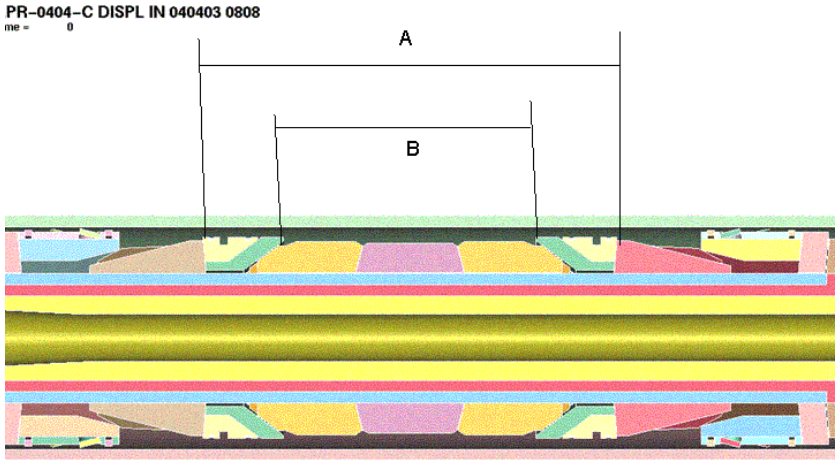

Figure 26. Close-up cross section of region of interest in 'as assembled' configuration

The corresponding view for the ‘deformed’ configuration is shown in Figure 27.

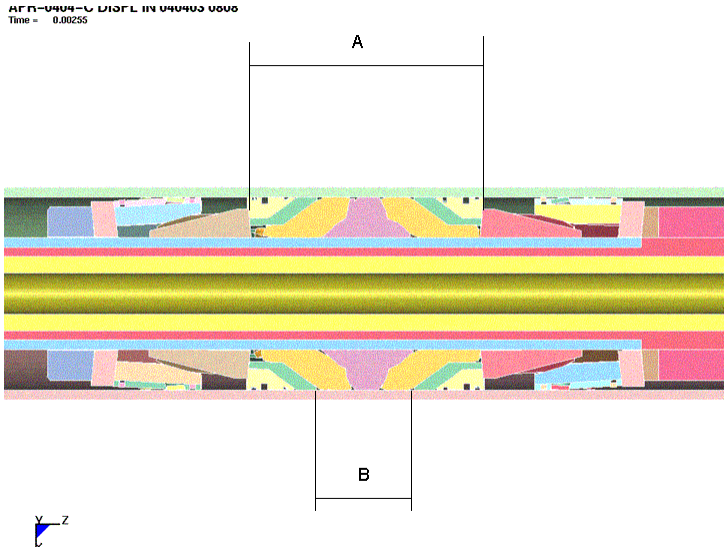

Figure 27. ‘Deformed’ configuration of cross section region of interest.

The ‘time-history’ of the parameters ‘A’ and ‘B’ described in Figures 26 and 27 is shown in Figures 28 and 29. The dimensions in these figures are inches and seconds for displacement and time respectively.

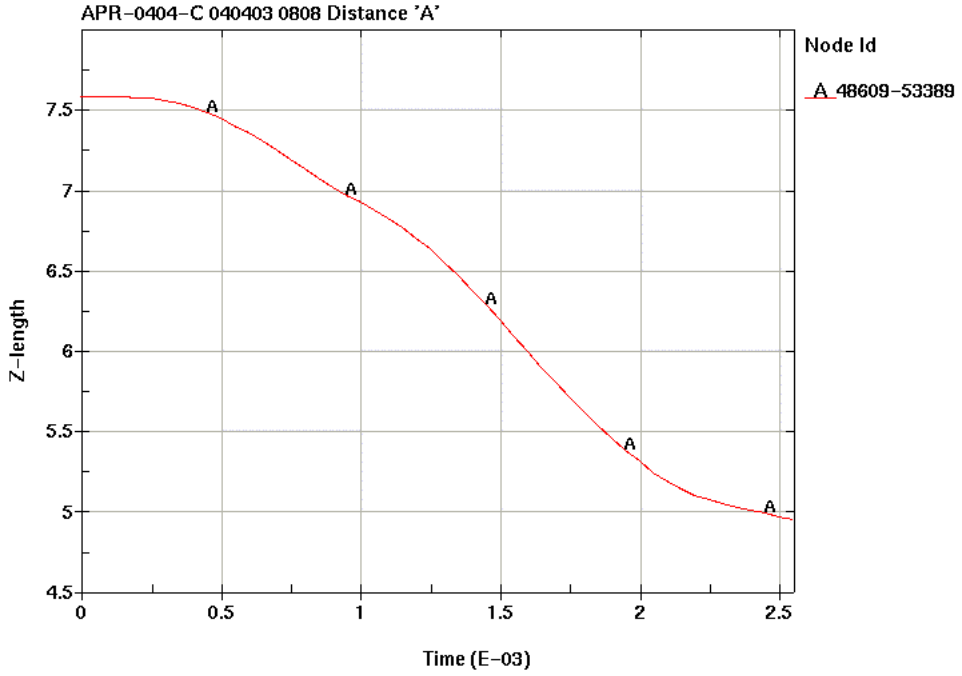

Figure 28. Time-history of distance between inner sides of wedges in the assembly.

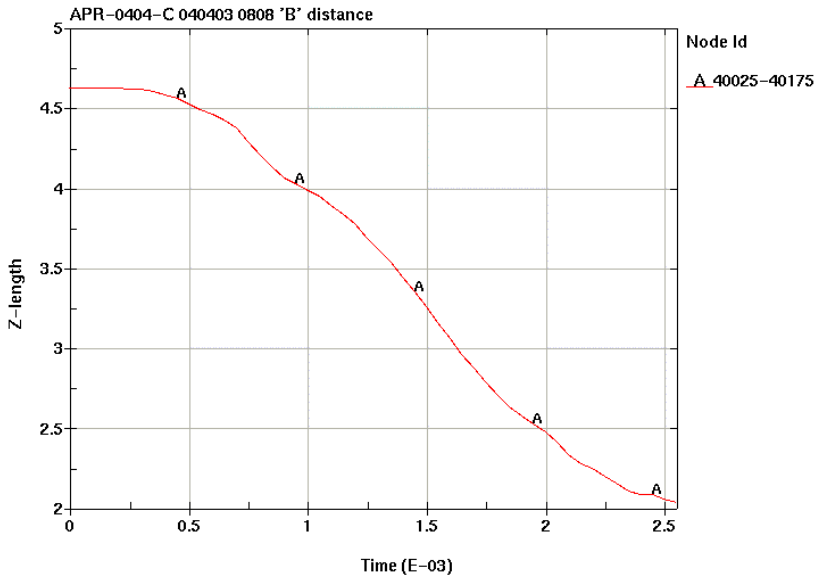

Figure 29. Time-history of distance between inner sides of extrusion limiters.

Table 1 presents a summary of results for the two different plug assembly configurations.

Table 1. Summary of Results

	Dwg CLO 803.94590 4.09" casing	**Finite Element Analysis**
'A' (inches)	4.825	4.95
'B' (inches)	1.859	2.04

Comparison of 'analysis' and 'experiment' is reasonable when one considers the extensive number of assumptions made in the analysis and the fact that the comparison is probably being made between two different plug configurations.

Additional results for this model were provided to Halliburton in a separate electronic document in the form of an avi file for viewing the dynamic motion of the bridge plug. Also provided in a separate document is the finite element input data used for running this analysis with LS-DYNA.

2.1.3 Material Properties

The CompositePro software program was used to estimate effective sets of material properties for the various components used in the finite element model. The first step in this process was to obtain properties for the different constituents. Typical isotropic properties were assumed for the epoxy resin system and vendor data sheets were referenced for the E-glass and S2-glass properties. The next step in the process was to estimate the transversely-isotropic properties of a unidirectional lamina. For both the E-

glass and S2-glass/epoxy systems a fiber volume fraction of 0.5 was assumed. Using the unidirectional lamina results, three sets of laminate properties were calculated, a 0/90 cross-ply set of properties for both the E-glass and S2-glass fiber reinforcements, and a +45/-45 set of properties for E-glass.

The next step was to use the fabric builder feature under the utilities pull-down menu in CompositePro. Five different sets of material properties were generated that corresponded to the different components modeled in the finite element analysis. Although there are more than five different material systems being considered for manufacturing the composite parts, it was felt that these calculated sets would provide an adequate representation of the various material systems and architectures. The warp-to-fill weight ratio and fiber orientation for the different braided systems considered were:

7781 Woven:	51:49	0/90
6781 Woven:	51:49	0/90
1543 Woven:	91:0	0/90
120 Woven:	50:50	0/90

For the CDB-120 stitched system the ply structure was 0/+45/-45. The last set of material properties to estimate was for the E-glass FM8130E molding compound. This system's properties were calculated assuming a random continuous mat architecture in CompositePro's fabric builder. The areal weight was iterated on to achieve the desired ply thickness. The results of all these calculations are summarized in Table 2. For parts that may be wet-filament wound, where the fiber orientations are all in the circumferential direction, unidirectional lamina properties with a fiber volume fraction of 0.70-0.75 can be used with a 90° rotation of the principal material directions, i.e., interchange the 1 and 2 subscripts. The subscript nomenclature in Table 2 refers to 1 as the direction parallel to the fiber reinforcement, 2 is perpendicular to the fiber direction, and 3 is perpendicular to the through-thickness (or out of plane) direction. Note, as a general rule micromechanics approaches do a reasonably good job of estimating material stiffness but material strengths that are used to predict failure should be experimentally determined.

Table 3 summarizes some of the experimental data that was provided by General Plastics and Composites for the braided material systems. In comparing these results with Table 2, it appears that the micromechanics approach underestimates the stiffness. However, in general, there is not a huge discrepancy between the two results and the property values shown in Table 2 should have sufficient accuracy for implementation in any finite element analyses where a complete set of consistent properties is required. Also, in reviewing the results in Table 2, as a first approximation for conducting a finite element analysis with composite parts, isotropic material behavior can be assumed with an elastic modulus equal to 3.0 Msi.

Table 2. Effective material properties

Material	E_1 (Msi)	E_2 (Msi)	E_3 (Msi)	ν_{12}	ν_{13}	ν_{23}	G_{12} (Msi)	G_{13} (Msi)	G_{23} (Msi)	ρ (lb/in^3)
Constituents										
Epoxy (resin)	0.620	0.620	0.620	0.3400	0.3400	0.3400	0.2300	0.2300	0.2300	0.04570
E-Glass (fiber)	10.500	10.500	10.500	0.2000	0.2000	0.2000	4.4000	4.4000	4.4000	0.09400
S2-Glass (fiber)	12.750	12.750	12.750	0.2000	0.2000	0.2000	5.1700	5.1700	5.1700	0.08900
Lamina										
E-Glass/Epoxy	5.560	1.853	1.853	0.2700	0.2700	0.3950	0.6069	0.6069	0.4371	0.06985
S2-Glass/Epoxy	6.685	1.894	1.894	0.2700	0.2700	0.4017	0.6178	0.6178	0.4404	0.06735
Laminate										
E-Glass 0/90	3.731	3.731	1.974	0.1346	0.3530	0.3530	0.6069	0.5220	0.5220	0.06985
S2-Glass 0/90	4.319	4.319	2.045	0.1189	0.3602	0.3602	0.6178	0.5291	0.5291	0.06735
E-Glass 45/-45	1.894	1.894	1.974	0.5606	0.1792	0.1792	1.6440	0.5220	0.5220	0.06895
Fabric										
E-Glass 7781 Woven	2.593	2.643	1.458	0.1500	0.4003	0.3976	0.4221	0.3769	0.3786	0.06150
S2-Glass 6781 Woven	3.055	3.122	1.538	0.1308	0.4076	0.4079	0.4370	0.3877	0.3896	0.06039
E-Glass CDB-200 Stitched	3.852	1.343	1.343	0.2942	0.2942	0.4540	0.4221	0.4221	0.3333	0.06150
E-Glass 120 Woven	2.618	2.618	1.458	0.1514	0.3990	0.3990	0.4221	0.3777	0.3777	0.06150
E-Glass 1543 Woven	1.573	3.637	1.386	0.1088	0.4454	0.3221	0.4221	0.3413	0.4141	0.06150
Molding Compounds										
E-Glass FM8130E	1.691	1.691	1.260	0.3355	0.3311	0.3311	0.6331	0.3298	0.3298	0.05752

For the molding compound system, experimental data found in material handbooks list stiffness values for glass-reinforced molding compounds that range from 1.2 to 2.4 Msi. This is at least consistent with the micromechanics estimate provided in Table 2. References to journal articles that discuss different micro-mechanics schemes for composites are provided below, as well as contact information for two software programs (including CompositePro) that can be used to calculate composite properties based on the constituent properties and composite architecture.

Table 3. Experimental data from General Plastics and Composites

Product	Material	E (Msi)	Notes
GP 301	7781 E-Glass	3.20	$V_f = 0.5$
GP 295		2.99	
GP 454		4.00	
GP 301	6781 S2-Glass	3.84	Estimated from the fiber modulus ratio: $E_{S2}/E_E = 1.2$
GP 295		3.59	
GP 454		4.80	

3. ACKNOWLEDGEMENTS

This work was supported by the 100% funds-in CRADA with Halliburton.

4. REFERENCES

Micromechanics References:

B. V. Sankar and R. V. Marrey, “Analytical Method for Micromechanics of Textile Composites,” Composites Science and Technology, Vol. 57, 1997, pp. 703-713.

D. Scida, Z. Aboura, M. L. Benzeggagh, and E. Bocherens, “A Micromechanics Model for 3D Elasticity and Failure of Woven-Fibre composite Materials,” Composites Science and Technology, Vol. 59, 1999, pp. 505-517.

Z. Huang, “The Mechanical Properties of Composites Reinforced with Woven and Braided Fabrics,” Composites Science and Technology, Vol. 60, 2000, pp. 479-498.

Micromechanics Software:

CPA: Composite Property Analysis
Center for Composite Materials, University of Deleware
Technical Contact: Prof. Rushad F. Eduljee
Phone: 302-831-8701
E-mail: eduljee@ccm.udel.edu

CompositePro
Peak Composite Innovations, LLC
Phone: 303-973-3032
E-mail: sales@compositepro.com
Web-site: http://www.compositepro.com

APPENDIX A. FINITE ELEMENT MODELS OF COMPONENTS

APPENDIX A
Finite Element Models of Components

The correspondence between the Part Number on the 'Part List' as provided by Halliburton for the Bridge Plug Assembly and the actual Finite Element model components used in the analysis is described in table A1 of this appendix.

Table A1. Part List-Finite Element Model Correspondence

Part No (1)	Ref. Drawing (1)	Description	Figure Number (2)
1	803.94501	Mandrel, Bridge Plug	**A1**
2	803-94504	Ring-Spacer	**A2**
3	803-94506	Ring-Slip Retaining	**A3**
5	803-94523	Wedge- HPHT- Extrusion Limiter	**A4**
6	803-94588	Ring Assembly- Extrusion Limiter- Segmented	**A5**
	803-94589		
7	803-94512	Rubber Set Packer	**A6**
7	802-30924	Rubber Set- Center	**A7**
7	803-94510	Rubber Set- End	**A8**
8	803-94507	Shoe- Mule	**A9**
9	803-94508	Plug- Bridging	**A10**
4	803-94514	Slip	**A11**
19	803-94511	Ring- Retaining	**A12**
-	803-94587	Ring- segmented, extrusion limiter- (outer)	**A13**
21	?	Mandrel- Inner	**A-14**
-	?	Ring Filler	**A-15**

(1) The part number and reference drawings are from the Halliburton Assembly list
(2) The figure numbers correspond to the finite element part use in the analysis

The figures that follow present the finite element developed parts used in this analysis.

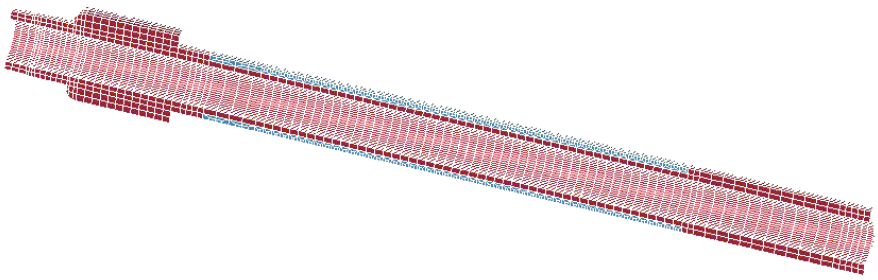

Figure A-1- Mandrel, Bridge Plug

Figure A1 displays the Mandrel Bridge Plug, the blue colored component in this figure corresponds to the region of the mandrel that interfaces the moving components of the assembly, and the mesh in this region is finer than the remaining part of the mandrel.

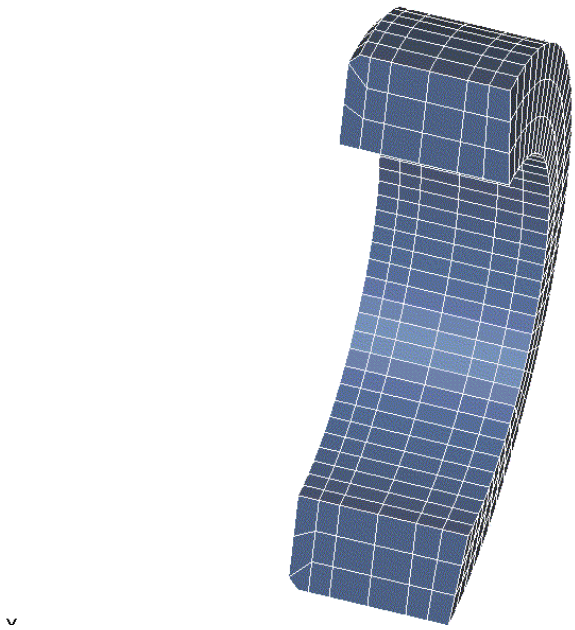

Figure A-2- Ring Spacer.

Figure A2 presents the ring spacer that provides the point of support to the moving assembly. The left side of the ring, in the figure, is constrained axially. The right side of the ring makes contact with the 'dummy' ring fillers that limit the amount of travel of the moving mandrel.

Figure A-3- Ring Slip retaining components.

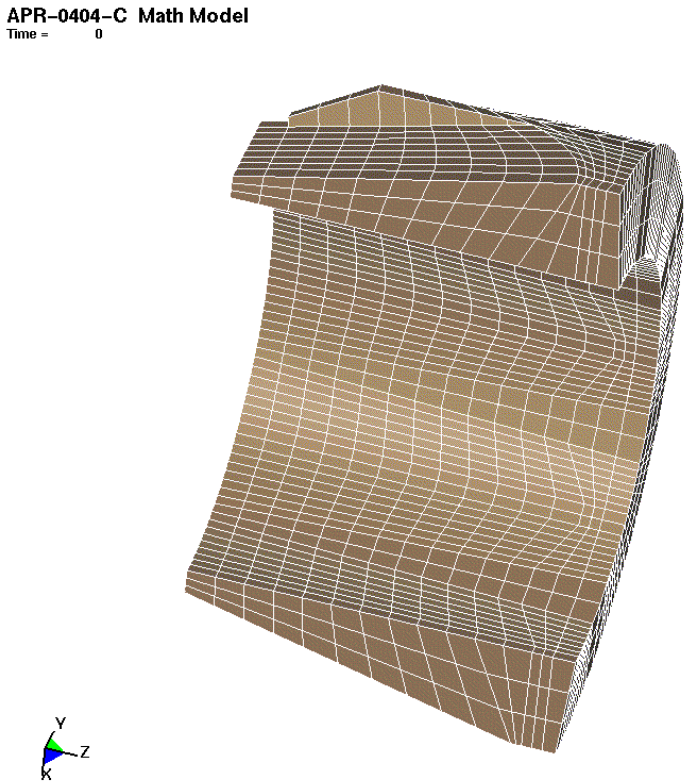

Figure A-4 Wedge HPT extrusion Limiter (left side component shown).

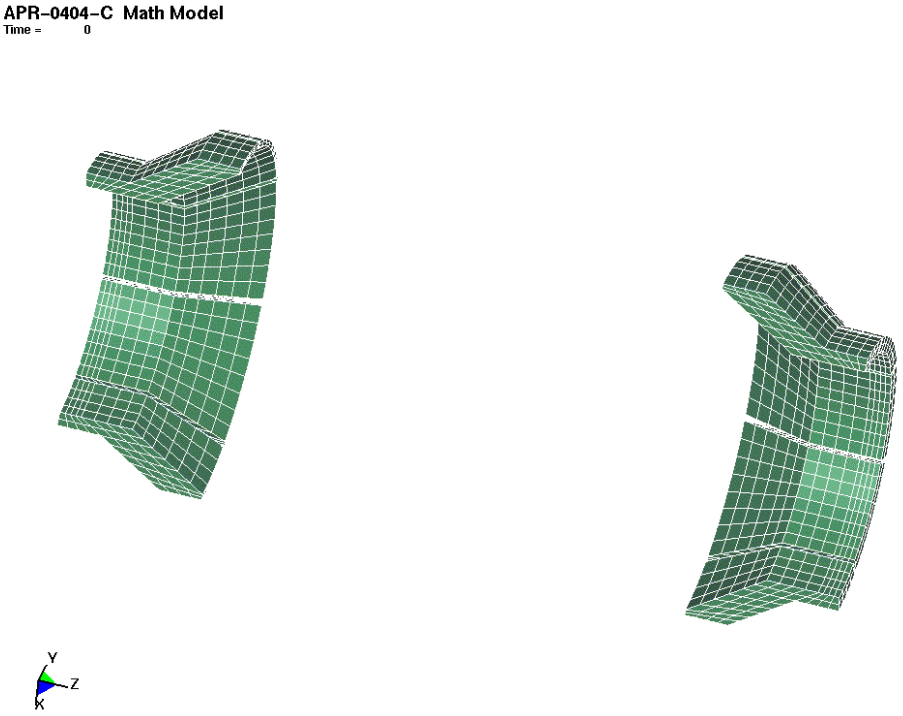

Figure A-5- Ring Assembly- Extrusion Limiter (inner component).

Figure A5 shows the inner part of the Ring assembly –extrusion limiter. The left and right side parts of this component are shown.

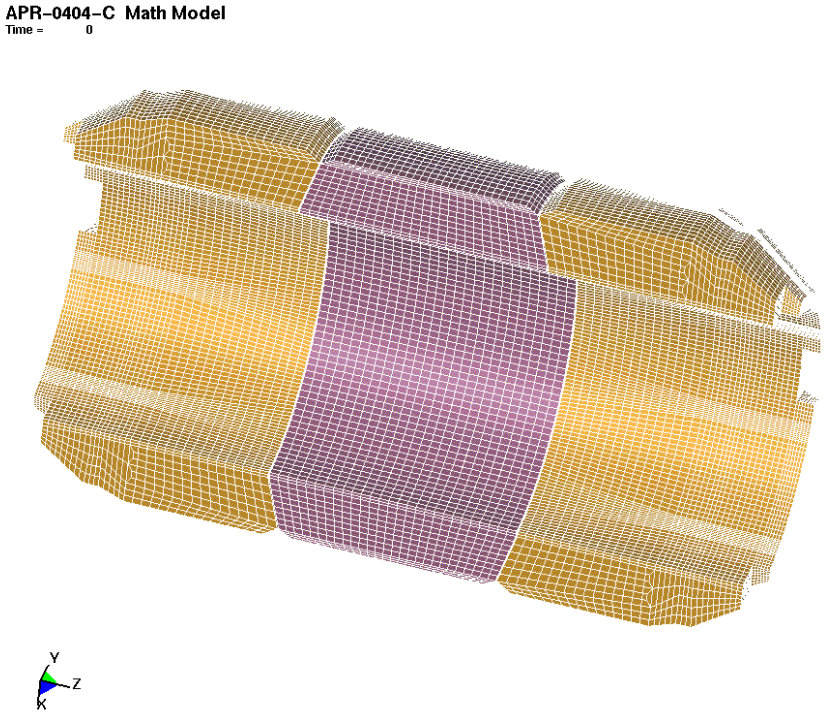

Figure A-6- Rubber Set Packer.

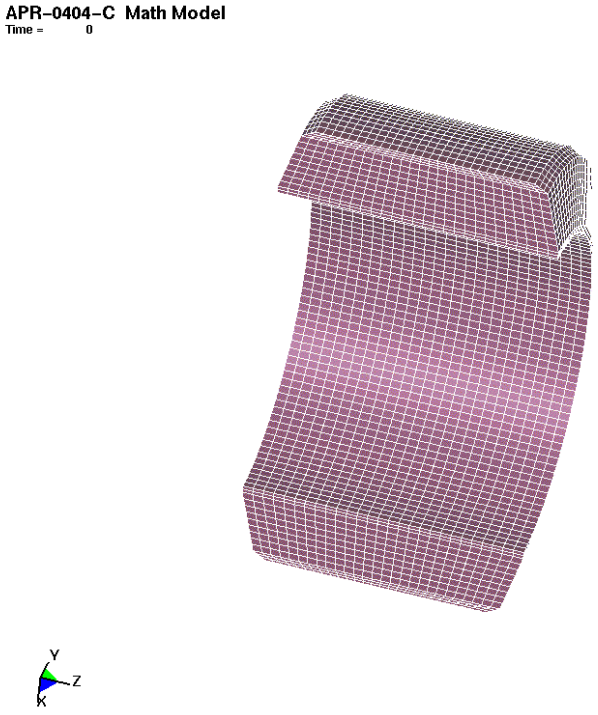

Figure A-7- Rubber Set Packer- Center part.

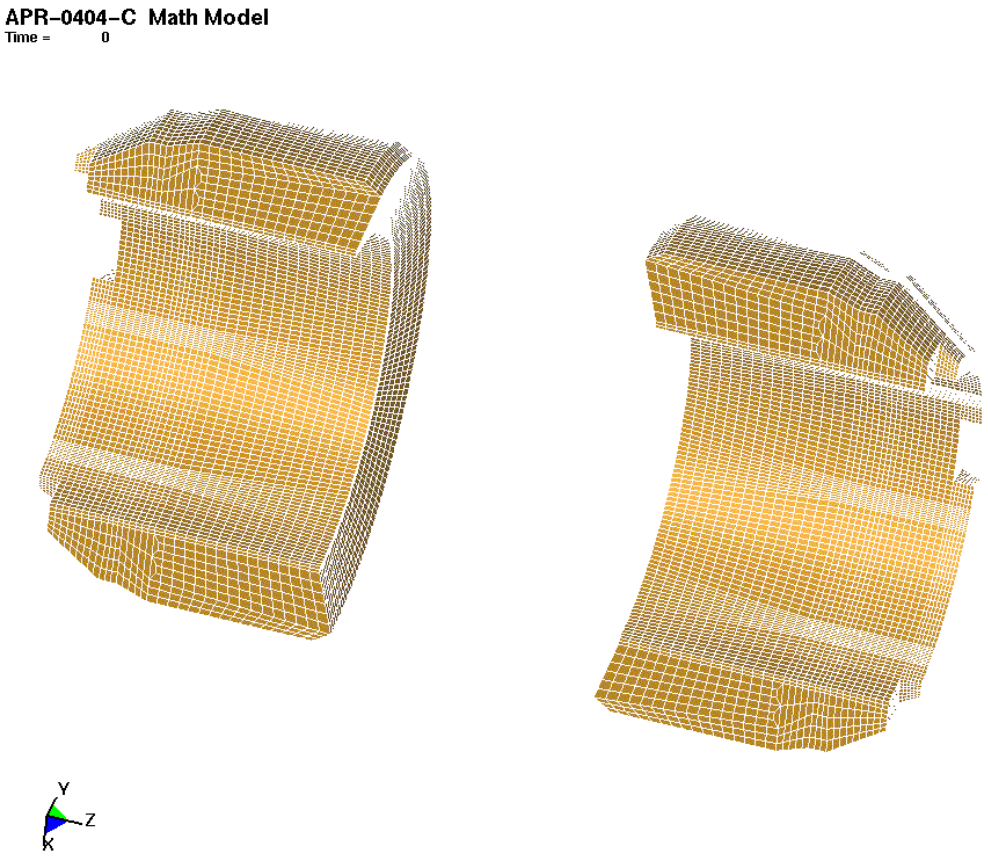

Figure A-8- Rubber Set packer- End parts.

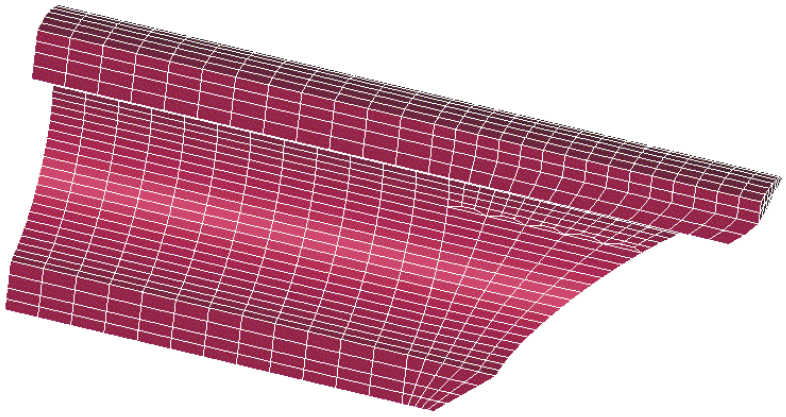

Figure A-9- Shoe- Mule.

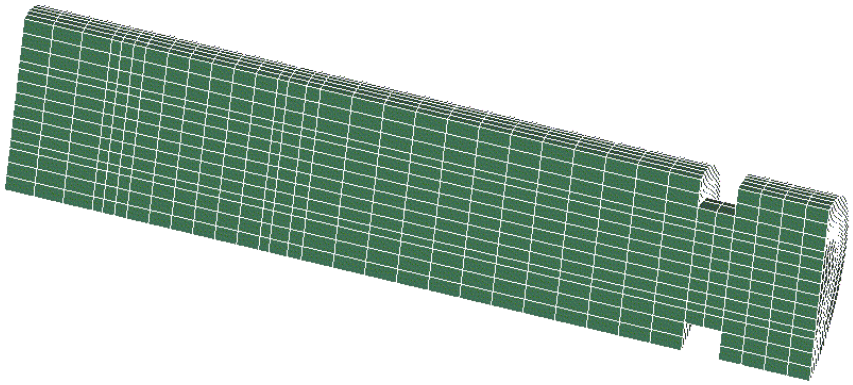

Figure A-10 Plug bridging.

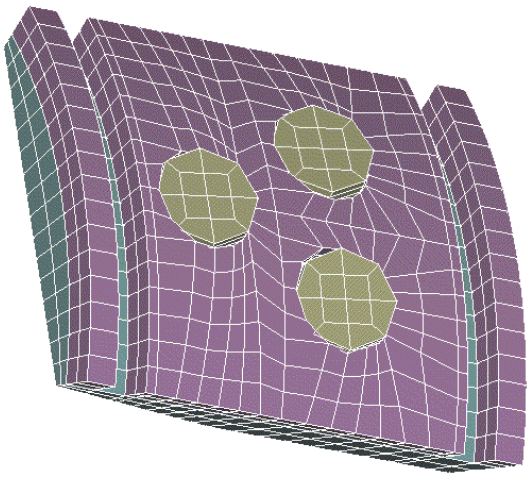

Figure A-11- Ring- segmented, extrusion limiter (outer),

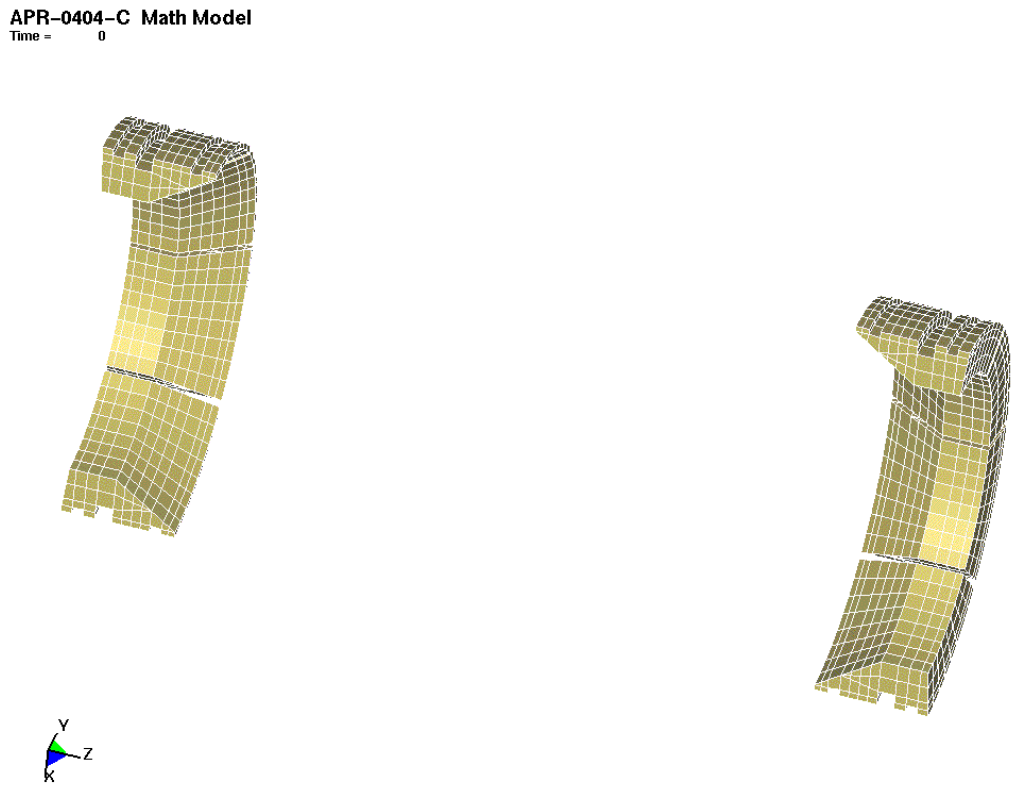

Figure A-13 Ring segmented extrusion limiter (outer).

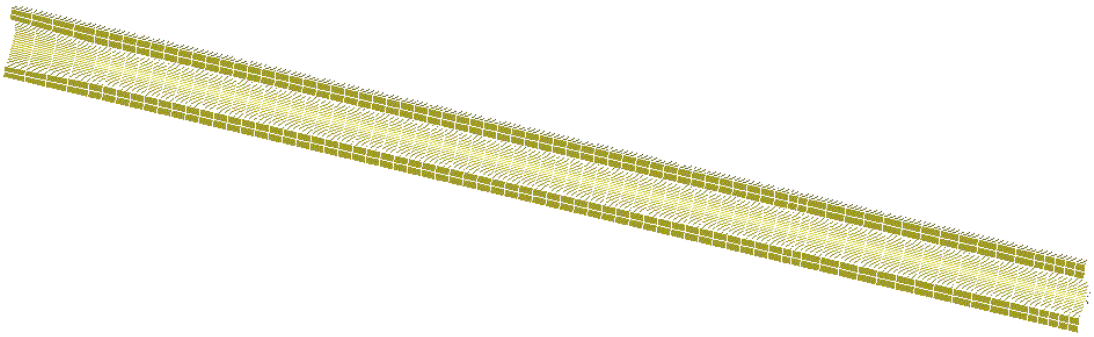

Figure A-14- Mandrel- Inner part.

Figure A-15- Dummy ring fillers.

Figure A-15 shows the ring fillers that have been placed to fill gaps in the Bridge Assembly. The assemblage of the finite parts described above is shown in Figure A-16 in a cut-away mode in the region of interest, and in a full mode for the entire package in Figure A-17

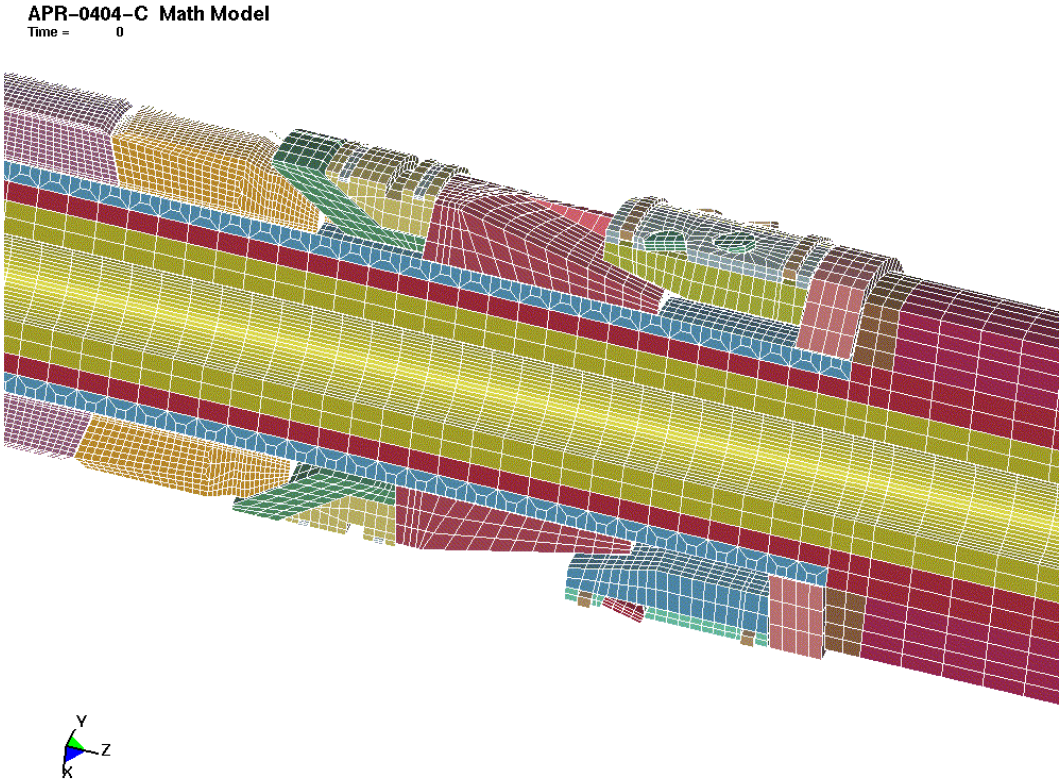

Figure A-16 Cut-away view of finite element model components.

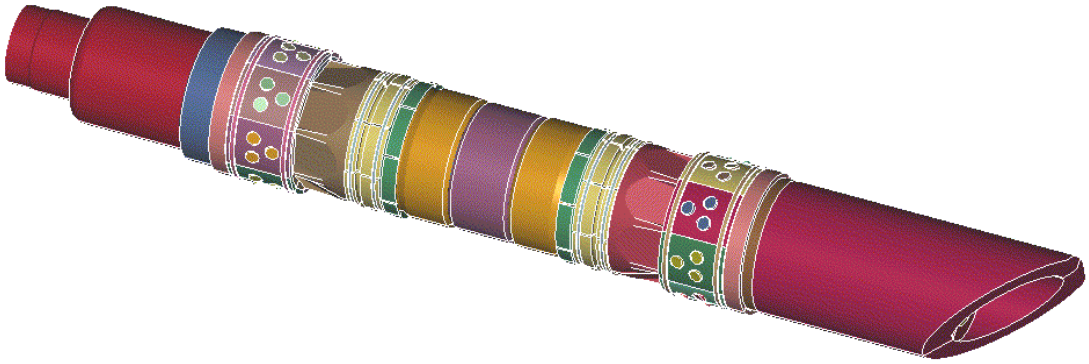

Figure A-17- reflected view of entire finite element model.

DISTRIBUTION

Internal

1. G. Aramayo
2. E. E. Bloom
3. C. R. Luttrell
4. R. E. Norris, Jr.
5. J. M. Starbuck
6. Kim Wilson
7. DOE-WFO
8. ORNL Site Office
9. ORNL Central Research Library
10. Office of Technical Information and Classification

External

Halliburton

1. Syed Hamid